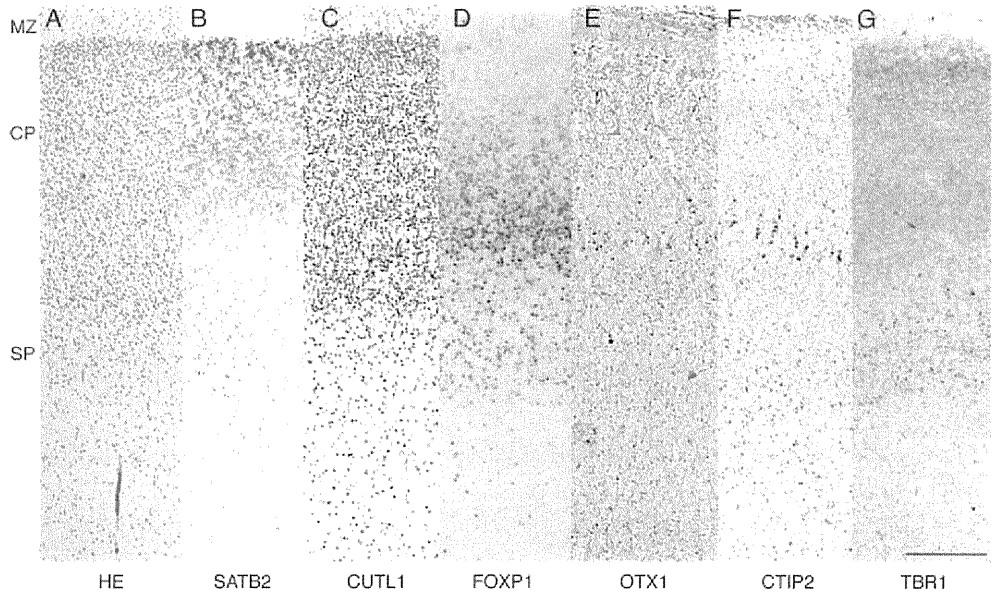

Figure 1. Layer-specific marker expression of the neocortex at 23 GWs. Around 20 GWs, the 3-layer pattern, that is, the marginal zone (MZ), CP, and subplate (SP), are seen (*A*). SATB2 expresses in the upper region of CP (*B*). CUTL1 diffusely expresses in the whole cortex and intermediate zone (*C*). FOXP1-positive cells locate in the middle region (*D*) and CTIP2-immunopositive cells (*F*) locate in the lower region of CP. OTX1 exhibits in CP and SP, predominantly lower region of CP (*E*). TBR1-immunopositive cells are in the lower region of CP and SP, as well as those fibers in CP (*G*). *A*, HE; *B–G*, SATB2, CUTL1, FOXP1, OTX1, CTIP2, and TBR1 immunohistochemistry, respectively. Scale bar: 100 μm.

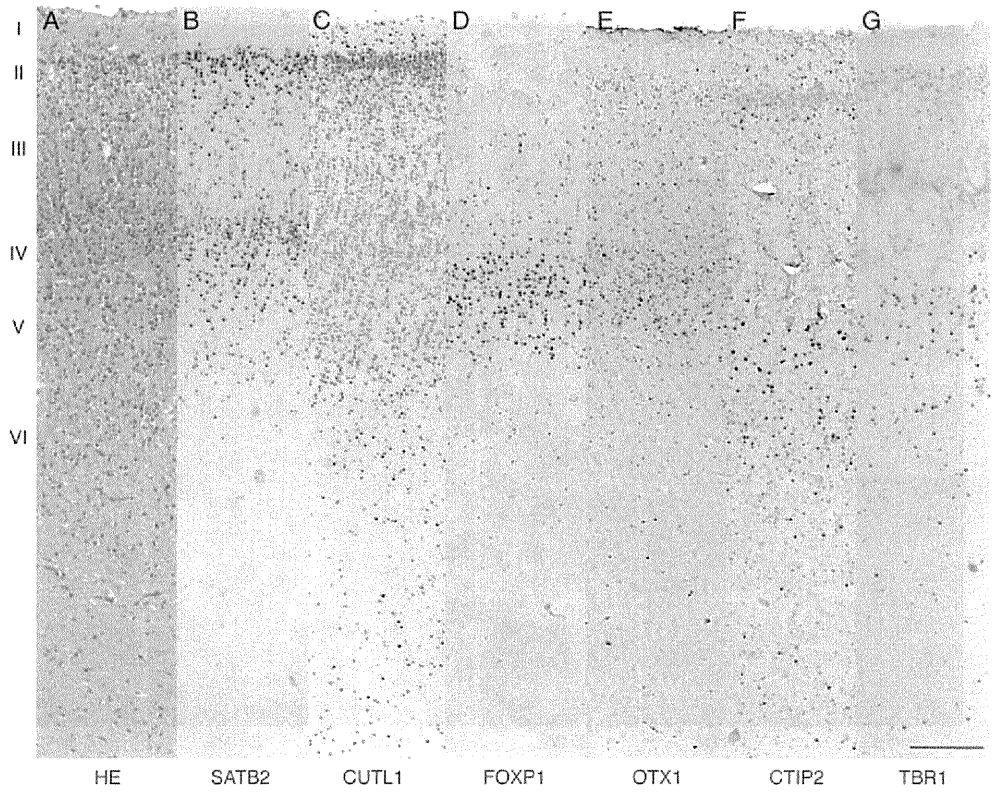

Figure 2. Layer-specific marker expression of the neocortex at 29 GWs. The 6-layer neocortex is shown (*A*). SATB2 expresses in layers II–V, especially layer II and upper region of layer IV (*B*). CUTL1 diffusely expresses in layers II–V and predominates in layer II (*C*). FOXP1 converges to layers VI and V (*D*). OTX expresses in upper layer and layers VI and V (*E*). CTIP2- and TBR1-immunopositive cells locate in layer V and layers V and VI (*F* and *G*). *A*, HE; *B-G*, SATB2, CUTL1, FOXP1, OTX1, CTIP2, and TBR1 immunohistochemistry, respectively. Scale bar: 100 μm.

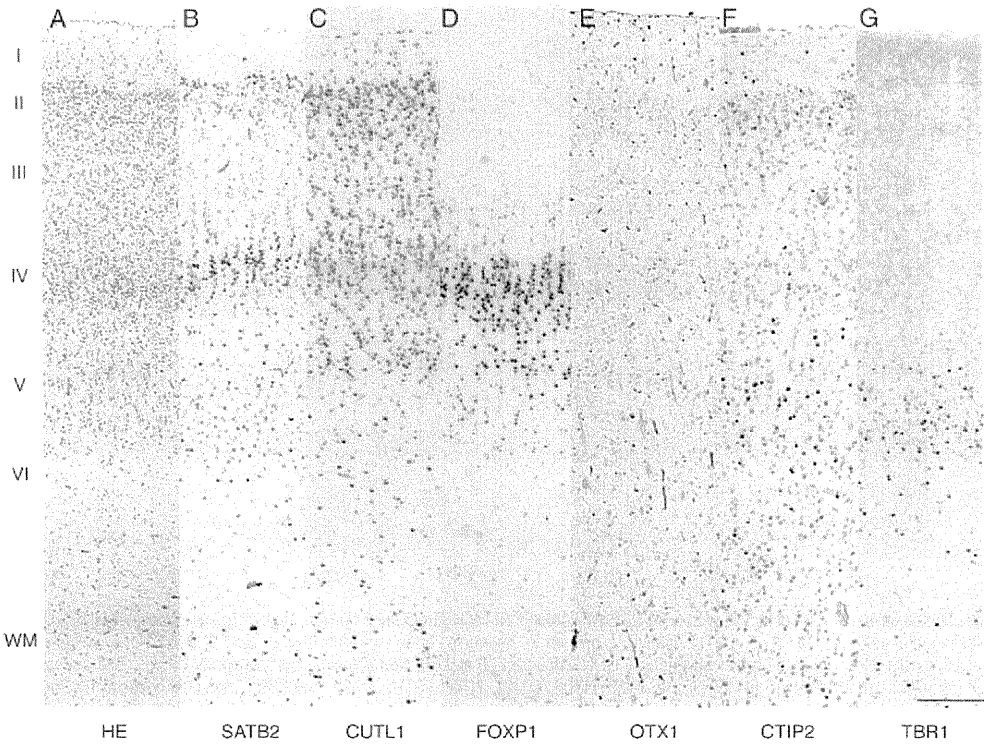

Figure 3. Layer-specific marker expression of the neocortex at 37 GWs. Expression of SATB2, CUTL1, FOXP1, OTX1, CTIP2, and TBR1 has a pattern similar to those at 29 GWs. OTX1 disappears in upper layer of neocortex (*E*). *A*, HE; *B–G*, SATB2, CUTL1, FOXP1, OTX1, CTIP2, and TBR1 immunohistochemistry, respectively. Scale bar: 100 μm.

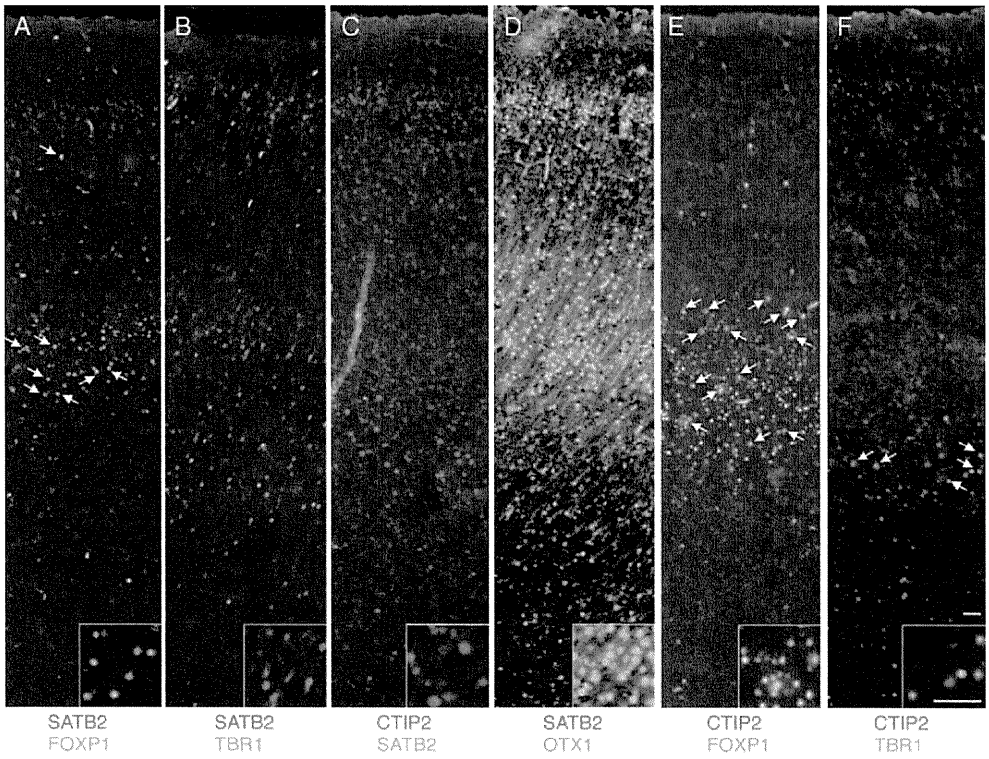

Figure 4. Immunofluorescence of layer-specific marker of neocortex at 29 GWs. FOXP1-immunopositive cells partially have SATB2 (merged color: arrows) in layers II–III and IV–V (*A*) and CTIP2 (merged color: arrows) in layers IV–VI (*E*). No double-positive cells for SATB2 and CTIP2 are scattered throughout all layers (*C*). No TBR1+ and SATB2+ cells are observed in layers V and VI (*B*), but a few TBR1+ and CTIP2+ cells are seen in layers V and VI (*F*). Many merged cells with SATB2 (red) and OTX1 (green) are diffusely demonstrated, predominantly in layers II and V (*D*). *A*, SATB2 (red) and FOXP1 (green) double fluorescence; *B*, SATB2 (red) and TBR1 (green); *C*, CTIP2 (red) and SATB2 (green); *D*, SATB2 (red) and OTX1 (green); *E*, CTIP2 (red) and FOXP1 (green); *F*, CTIP2 (red), and TBR1 (green). Scale bars: 20 μm.

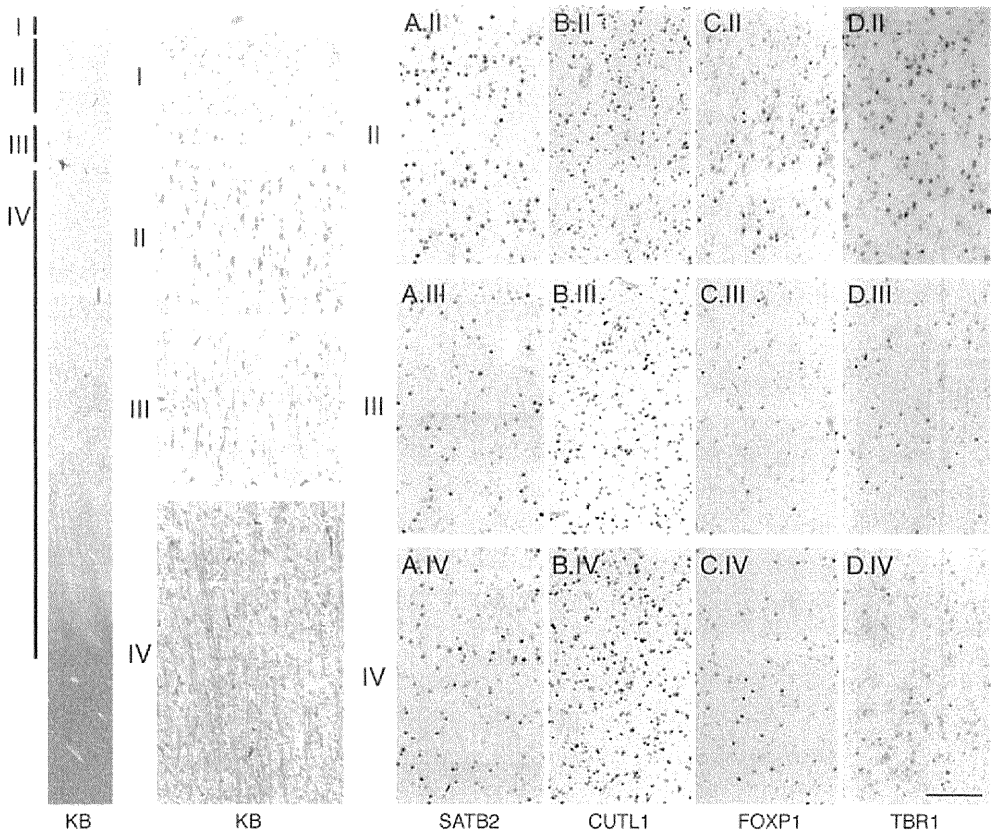

Figure 5. Layer-specific marker expression of the neocortex of 1-year-old patient with Miller–Dieker syndrome. Typical 4-layer pattern is shown. (*A*) SATB2, CUTL1, FOXP1, and TBR1 are diffusely expressed in layers II, III, and IV. Especially, TBR1-immunopositive cells locate in layer II (*E*). Enlargement of layer II shows *A.II*, *B.II*, *C.II*, and *D.II*. Enlargement of layer III shows *A.III*, *B.III*, *C.III*, and *D.III*. Enlargement of layer IV shows *A.IV*, *B.IV*, *C.IV*, and *D.IV*. Gross histology shows with KB staining. *A.II*, *A.III*, and *A.IV*, SATB2 in layers II, III, and IV; *B.II*, *B.III*, and *B.IV*, CUTL1; *C.II*, *C.III*, and *C.IV*, FOXP1; *D.II*, *D.III*, and *D.IV*, TBR1, respectively. Scale bar: 100 μm.

neurons (layer II), and a deep layer (layer III) (Fig. 6*A*). SATB2+ and CUTL1+ cells located in the intermediate layer and upper region of the deep layer (Fig. 6*B,C*). FOXP1+ cells and TBR1+ cells were also distributed in layer II and III (Fig. 6*D,E*). These labeled cells in the deep intermediate layer were large and dense but small and sparse in the upper region of the intermediate layer. Also, in the molecular layer, FOXP1+ and TBR1+ cells were few. No CTIP2+ and OTX1+ cells were observed in either malformed brain.

Usually, FCMD cerebral cortices show type II lissencephaly with cobblestone cortex. The cerebral cortices of FCMD fetus already revealed typical cobblestone lissencephaly (Fig. 7*A*). Neurons of the fetal neocortex migrated over the glia limitans. SATB2+, CULT1+, FOXP1+, CTIP2+, and TBR1+ cells were dense above the glia limitans and sparse below it (Fig. 7*B–D*), and TBR1+ cells were distributed predominantly below the glia limitans (Fig. 7*E*). However, no markers were detected in specimens from postnatal FCMD brains (data not shown).

The layer-specific marker expression pattern of 3 types of lissencephalies was summarized in Supplementary Figure 2.

Discussion

Very little is known about the molecular mechanism of human neocortex layer formation. Here, we presented new knowledge regarding the layer-specific marker expression in fetus development. Recent neuronal developmental studies have introduced some molecules as layer-specific markers. Among them, Satb2, Cutl1, Foxp1, Otx1, Ctip2, and Tbr1 are well-known transcriptional factors and highly conserved. The facts that SATB2 was relatively limited to layers II and IV of human fetus cortex and that Cutl1 was not known in human but was expressed in layers II–IV evidenced the same expression patterns of these molecules in rodent study (Nieto et al. 2004; Britanova et al. 2008). The migration pattern of callosal projection neurons may be the same as that in the mouse. FOXP1+ cells located in deep layers or layers IV–V before 30 GW and in layers IV–VI before birth. TBR1+ cells located in layers V–VI in the fetal period. FOXP1+ and TBR1+ cell localization in layers IV and V was similar to those in a previous human study (Sheen et al. 2006). However, TBR1+ cells were located beneath FOXP1+ cells but not colocalized. The restricted distribution of CTIP2+ cells in layer V may reflect the corticospinal projection formation, as indicated by mouse *ctip2* analysis (Arlotta et al. 2005). Interestingly, SATB2+ cells were located in the upper region of layer IV and FOXP1+ cells in the lower region of the same layer. This different localization indicates completely different neural functions between SATB2 and FOXP1, although the FOXP1 function in neocortex is unknown.

In mouse neocortex, Otx1+, Tbr1+, Ctip2+, Foxp1+, Cutl1+, and Satb2+ neurons are born around embryonic day 12.5, 10.0,

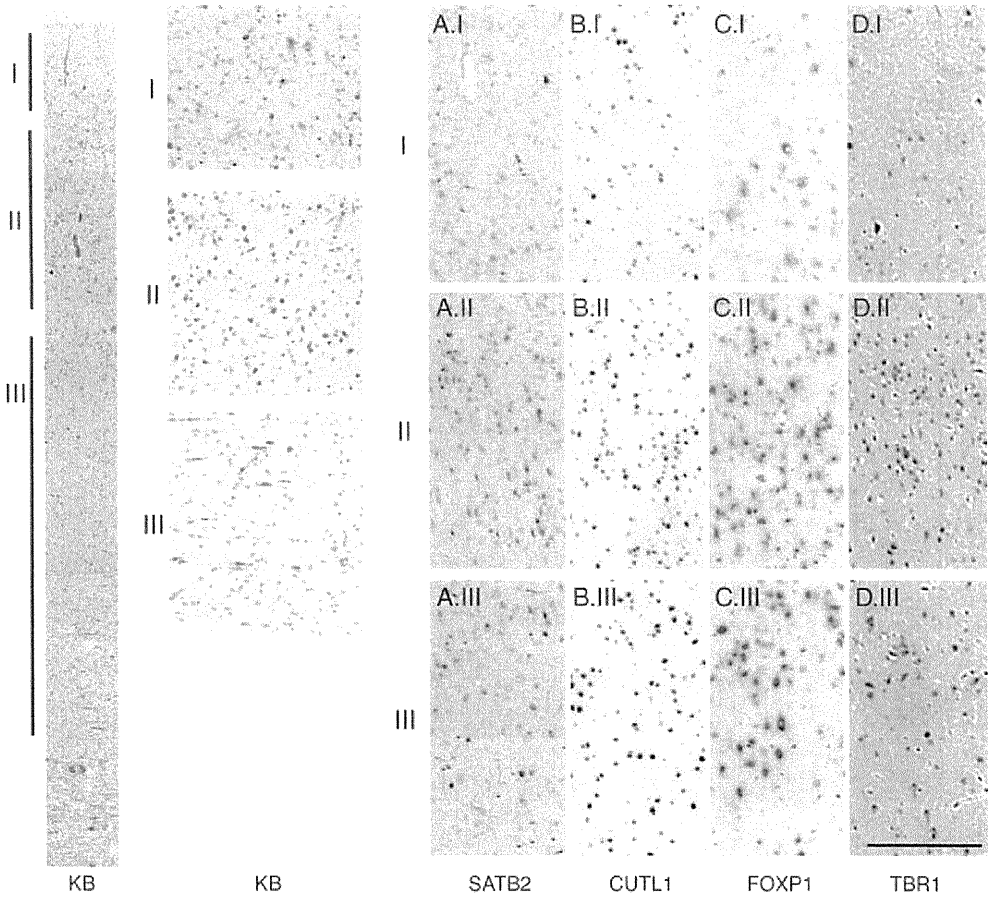

Figure 6. Layer-specific marker expression of the neocortex of 10-month-old boy with XLAG. Neocortex shows a thin 3-layer pattern. SATB2-, CUTL1-, FOXP1-, and TBR1-immunopositive cells locate diffusely (*A–D*). Gross histology shows with KB staining. *A.I*, *A.II*, and *A.III*, SATB2 in layers I, II, and III; *B.I*, *B.II*, and *B.III*, CUTL1; *C.I*, *C.II*, and *C.III*, FOXP1; *D.I*, *D.II*, and *D.III*, TBR1, respectively. Scale bar: 100 μm.

12.0, 14.5, 13.0, and 13.5, respectively (Simeone et al. 1993; Bulfone et al. 1995; Hevner et al. 2001; Ferland et al. 2003; Leid et al. 2004; Nieto et al. 2004; Arlotta et al. 2005; Britanova et al. 2005). These labeling neurons originate from progenitor cells residing in the ventricular zone (VZ) and the subventricular zone (SVZ) of early developing brain. Early progenitor cells in VZ produce deep layer neurons expressing Ctip2. On the contrary, late progenitor cells in SVZ form upper layers, expressing Cutl1 (Nieto et al. 2004). The previous data that Satb2-null mice show loss of Cutl1+cells in the superficial layers (Alcamo et al. 2008) suggest the profound molecular relationship of Satb2 and Cutl1. Satb2+ cells directly contribute to the formation of a callosal projection of the bilateral neocortical connection (Alcamo et al. 2008), while Ctip2+ cells contribute to the formation of a corticospinal projection forming a long pathway between the neocortex and anterior horn of the spinal cord (Arlotta et al. 2005). Interestingly, the expression patterns of SATB2 and CTIP2 in human neocortex mimicked those of rodent, and SATB2+ cells were also found in part of layer V. Although SATB2+ cells and CTIP2+ cells were in layer V, these double-marked cells were not observable. This may indicate these cells have different functions. From rodent study, 2 major projection neurons, callosal and subcortical, are formed by Satb2 and Ctip2 interaction (Leone et al. 2008), which may be at work in the human fetal neocortex. The finding of no double-labeled cells with CTIP2 and SATB2 in human neocortex is compatible with the rodent data (Leone et al. 2008). Otx1 in mouse brain also expresses in layer V and contributes to the formation of the corticospinal projection (Frantz et al. 1994; Weimann et al. 1999). CTIP2+/OTX1+ cells may be closely related to the forming of the corticospinal projection. Interestingly, we found many SATB2+/OTX1+ cells in layer V. OTX1 may play an essential role in the specification of both callosal and corticospinal projection neurons, although the detailed interaction between OTX1 and CTIP2 remains unknown. Moreover, FOXP1+ cells expressed SATB2 and CTIP2 in layer V. It is unknown whether a relationship exists between Foxp1 and Satb2 or Foxp1 and Ctip2, although Ctip2 is known to colocalize with Foxp1 in mouse striatum (Arlotta et al. 2008). FOXP1 may also contribute callosal and corticospinal projection neurons. FOXP1 disappeared earlier than OTX1 (Figs 2 and 3 and Supplementary Figure 1). FOXP1 could strongly control forming corticospinal projection. Tbr1+ cells derived from the earliest progenitor cells locate in layer VI (Hevner et al. 2003) and contribute to the development of corticothalamic projection neurons (Hevner et al. 2001, 2002; Guillemot et al. 2006; Leone et al. 2008). In our data, the TBR1+ cells that expressed CTIP2 in layer VI may form corticothalamic projections, as in rodent studies.

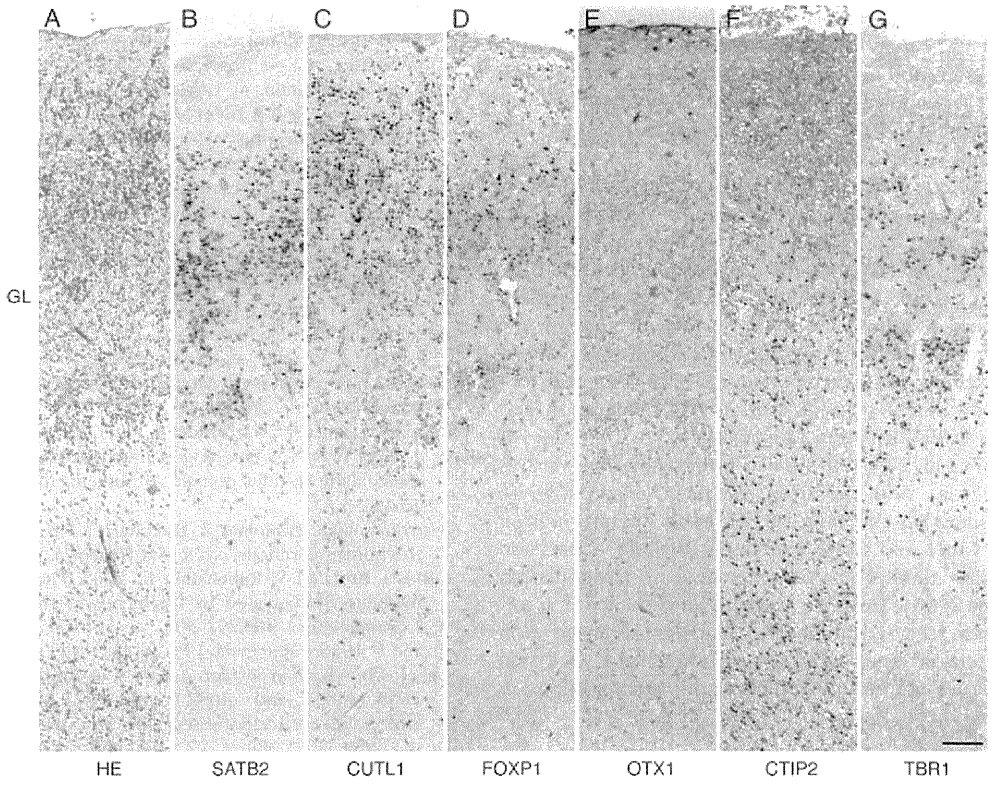

Figure 7. Layer-specific marker expression of the neocortex of 19-GW fetus with FCMD. Neocortex shows typical cobblestone lissencephaly feature. Many SATB2-, CUTL1-, FOXP1-, OTX1, CTIP2-, and TBR1-immunopositive cells migrate over the glia limitans (*B–G*), while some labeled cells locate under it. GL, glia limitans; *A*, HE; *B–G*, SATB2, CUTL1, FOXP1, OTX1, CTIP2, and TBR1 immunohistochemistry, respectively. Scale bar: 100 μm.

On the other hand, malformed neocortices revealed unique distributions of the layer-specific markers. In MDS, due to deletion of 17p13.3 with LIS1 gene, it has been thought that neurons of the superficial layer are neuronal components of the fundamental deep layers, and neurons of the deep layers consist of neuronal components of layers II–IV in the normal neocortex (Ferrer et al. 1987). Also, MDS neocortical lamination was found to have an inverted organization (Viot et al. 2004). However, recently the neocortex of 33 GW MDS has reportedly demonstrated FOXP1+ cell in the deep layers or TBR1+ cells in the first 3 layers (Sheen et al. 2006). MDS neocortical lamination was concluded to be preserved and noninverted. Our MDS findings supported noninverted lamination because of the diffuse expression pattern of all layer-specific markers. XLAG, caused by loss of function mutations of ARX gene concerned with differentiation and migration of γ-aminobutyric acidergic interneurons, shows a 3-layer lissencephalic neocortex (Kitamura et al. 2002; Bonneau et al. 2002; Cobos et al. 2005; Forman et al. 2005). Although ARX-null mice exhibit nearly normal layer formation of the cerebral cortex (Kitamura et al. 2002), the human XLAG neocortex was reported to consist of 3 layers with uniform pyramidal neurons (Bonneau et al. 2002; Okazaki et al. 2008). From our observation of layer-specific markers in layers II and III, XLAG might also be a random migration pattern. In human brain, ARX involves migration of not only interneurons but also projection neurons (Okazaki et al. 2008). XLAG neocortex may have an abnormal interneuron migration pattern, although in the present study this could not be demonstrated. Interestingly, our postnatal patients with MDS and XLAG revealed persistent expression of these layer-specific markers, which was not found in the normal neocortex. This suggests that MDS or XLAG neurons arrest in the premature or undifferentiated stage.

Further investigation is needed to determine why these layer-specific markers are expressed in postnatal brains, and the nature of their molecular function. Moreover, we investigated neocortices of typical type II lissencephaly, FCMD. Various-sized and/or disoriented neurons were widely scattered in the neocortex. In FCMD fetal brain, the layer-specific markers diffusely expressed over and under glia limitans (Fig. 7). Obviously, the FCMD fetal neocortex had completely lost its layer formation. The layer-formation pattern of WWS fetus presents the same result as ours (Hevner 2007). This type II lissencephaly, cobblestone lissencephaly, may commonly have this pathological construction. Postnatal FCMD demonstrated no expression of the layer-specific markers and was different from MDS and XLAG. Neuronal maturation of FCMD neocortex may be more advanced than other types of lissencephalies. This leads us to conclude that FCMD patients have a relatively low incidence of epilepsy and some cases are mild (Guerrini and Filippi 2005; Spalice et al. 2009).

Our study suggests that the laminar formation pattern of human and rodent neocortices is fundamentally the same. One of the characteristics of the human neocortex is its gyration, which is 1000-fold in the neocortical surface area between human and rodent (Bystron et al. 2006; Rakic 2009). It is thought that not only the number of neuronal progenitors but also the number of radial glial cells in human brain is much

larger than in the rodent. As a result, the human neocortex must fold and form gyrations. However, in case of abnormal expression of migration- or proliferation-related genes or environments such as trauma and infection, the number of neuronal progenitor cells, and radial glial cells may serve to reduce and influence the migration pattern.

We may conclude that the neocortex of lissencephalies is formed by a unique type of neuronal migration. The late-birth cells in MDS may migrate randomly but not the early-birth cells. In XLAG, SATB2+, and TBR1+ cells distribute in the relatively deep layers, but CUTL1+ and FOXP1+ cells may follow a random migration pattern. FCMD shows the most random pattern. We must seek to understand the mechanism behind these differences. The molecular mechanism of neuronal movement is well known. Lis-1 or Dcx is a modulator of radial migration and contributes to layer formation (Hirotsune et al. 1998; Meyer et al. 2002; Bai et al. 2003). In human layer formation, various projection neurons originate from VZ or SVZ and migrate radially depending on the time of cell birth. In interneuron development, Cutl1 and Cutl2 contribute to Reln expression and control the number of the interneuron subpopulation (Cubelos et al. 2008). However, little is known about interaction between the layer-specific markers (transcription factors) and neuron kinetic factors including Lis-1, Dcx and Reln. Further study is warranted to obtain more information in this regard.

Supplementary Material

Supplementary material can be found at: http://www.cercor.oxfordjournals.org/.

Funding

Ministry of Health, Labor and Welfare of Japan (Intramural Research Grant [21B-5] for Neurological and Psychiatric Disorders of NCNP, and Research on Intractable Diseases 21-110 and 22-133 to M.I.).

Notes

We thank Drs M. Morikawa, Tokyo Metropolitan Kiyose Children's Hospital, B. Akikusa, Matsudo Municipal Hospital, and H. Horie, Chiba Children's Hospital, for advice on the pathology in this study, and Dr K. Kitamura, National Center of Neurology and Psychiatry, for helpful comments on the manuscript. We are also indebted to Mrs Y. Shono, Tokyo Metropolitan Hachioji Hospital, and Mr S. Kumagai, National Center of Neurology and Psychiatry, for technical assistance. *Conflict of Interest*: None declared.

References

Alcamo EA, Chirivella L, Dautzenberg M, Dobreva G, Fariñas I, Grosschedl R, McConnell SK. 2008. Satb2 regulates callosal projection neuron identity in the developing cerebral cortex. Neuron. 57:364–377.

Arlotta P, Molyneaux BJ, Chen J, Inoue J, Kominami R, Macklis JD. 2005. Neuronal subtype-specific genes that control corticospinal motor neuron development in vivo. Neuron. 45:207–221.

Arlotta P, Molyneaux BJ, Jabaudon D, Yoshida Y, Macklis JD. 2008. Ctip2 controls the differentiation of medium spiny neurons and establishment of the cellular architecture of the striatum. J Neurosci. 28:622–632.

Assadi AH, Zhang G, Beffert U, McNeil RS, Renfro AL, Niu S, Quattrocchi CC, Antalffy BA, Sheldon M, Armstrong DD, et al. 2003. Interaction of reelin signaling and Lis1 in brain development. Nat Genet. 35:270–276.

Bai J, Ramos RL, Ackman JB, Thomas AM, Lee RV, LoTurco JJ. 2003. RNAi reveals doublecortin is required for radial migration in rat neocortex. Nat Neurosci. 6:1277–1283.

Bonneau D, Toutain A, Laguerrière A, Marret S, Saugier-Veber P, Barthez MA, Radi S, Biran-Mucignat V, Rodriguez D, Gélot A. 2002. X-linked lissencephaly with absent corpus callosum and ambiguous genitalia (XLAG): clinical, magnetic resonance imaging, and neuropathological findings. Ann Neurol. 51:340–349.

Britanova O, Akopov S, Lukyanov S, Gruss P, Tarabykin V. 2005. Novel transcription factor Satb2 interacts with matrix attachment region DNA elements in a tissue-specific manner and demonstrates cell-type-dependent expression in the developing mouse CNS. Eur J Neurosci. 21:658–668.

Britanova O, de Juan Romero C, Cheung A, Kwan KY, Schwark M, Gyorgy A, Vogel T, Akopov S, Mitkovski M, Agoston D, et al. 2008. Satb2 is a postmitotic determinant for upper-layer neuron specification in the neocortex. Neuron. 57:378–392.

Bulfone A, Smiga SM, Shimamura K, Peterson A, Puelles L, Rubenstein JL. 1995. T-brain-1: a homolog of Brachyury whose expression defines molecularly distinct domains within the cerebral cortex. Neuron. 15:63–78.

Bystron I, Rakic P, Molnar Z, Blackmore C. 2006. The first neurons of the human cerebral cortex. Nat Neurosci. 9:880–885.

Cobos I, Broccoli V, Rubenstein JL. 2005. The vertebrate ortholog of Aristaless is regulated by Dlx genes in the developing forebrain. J Comp Neurol. 483:292–303.

Crome L. 1956. Pachygyria. J Pathol Bacteriol. 71:335–352.

Cubelos B, Sebastian-Serrano A, Kim S, Redondo JM, Walsh C, Nieto M. 2008. Cux-1 and cux-2 control the development of reelin expressing cortical interneurons. Dev Neurobiol. 68:917–925.

De Rouvroit CL, Goffinet AM. 2001. Neuronal migration. Mech Dev. 105:47–56.

Dobyns WB, Berry-Kravis E, Havernick NJ, Holden KR, Viskochil D. 1999. X-linked lissencephaly with absent corpus callosum and ambiguous genitalia. Am J Med Genet. 86:331–337.

Ferland RJ, Cherry TJ, Preware PO, Morrisey EE, Walsh CA. 2003. Characterization of Foxp2 and Foxp1 mRNA and protein in the developing and mature brain. J Comp Neurol. 460:266–279.

Ferrer I, Fábregues I, Condom E. 1987. A Golgi study of the sixth layer of the cerebral cortex. III. Neuronal changes during normal and abnormal cortical folding. J Anat. 152:71–82.

Forman MS, Sguler W, Dobyns WB, Golden JA. 2005. Genotypically defined lissencephalies show distinct pathologies. J Neuropathol Exp Neurol. 64:847–857.

Frantz GD, Weimann JM, Levin ME, McConnell SK. 1994. Otx1 and Otx2 define layers and regions in developing cerebral cortex and cerebellum. J Neurosci. 14:5725–5740.

Guerrini R, Filippi T. 2005. Neuronal migration disorders, genetics, and epileptogenesis. J Child Neurol. 20:287–299.

Guillemot F, Molnár Z, Takabykin V, Stoykova A. 2006. Molecular mechanisms of cortical differentiation. Eur J Neurosci. 23:857–868.

Hevner RF. 2007. Layer-specific markers as probes for neuron type identity in human neocortex and malformations of cortical development. J Neuropathol Exp Neurol. 66:101–109.

Hevner RF, Miyashita-Lin E, Rubenstein JLR. 2002. Cortical and thalamic axon pathfinding defects in Tbr1, Gbx2, and Pax6 mutant mice: evidence that cortical and thalamic axons interact and guide each other. J Comp Neurol. 447:8–17.

Hevner RF, Neogi T, Englund C, Daza RAM, Fink A. 2003. Cajal-Retius cells in the mouse: transcription factors, neurotransmitters, and birthdays suggest a pallial origin. Brain Res Dev Brain Res. 141:39–53.

Hevner RF, Shi L, Justice N, Hsueh Y, Sheng M, Smiga S, Bulfone A, Goffinet AM, Campagnoni AT, Rubenstein JL. 2001. Tbr1 regulates differentiation of the preplate and layer 6. Neuron. 29:353–366.

Hirotsune S, Fleck MW, Gambello MJ, Bix GJ, Chen A, Clark GD, Ledbetter DH, McBain CJ, Wynshaw-Boris A. 1998. Graded reduction of Pafah1b1 (Lis1) activity results in neuronal migration defects and early embryonic lethality. Nat Genet. 19:333–339.

Kitamura K, Yanazawa M, Sugiyama N, Miura H, Iizuka-Kogo A, Kusaka M, Omichi K, Suzuki R, Kato-Fukui Y, Kamiirisa K, et al.

2002. Mutation of ARX causes abnormal development of forebrain and testes in mice and X-linked lissencephaly with abnormal genitalia in humans. Nat Genet. 32:359–369.
Leid M, Ishmael JE, Avram D, Shepherd D, Fraulob V, Dollé P. 2004. CTIP1 and CTIP2 are differentially expressed during mouse embryogenesis. Gene Expr Patterns. 4:733–739.
Leone DP, Srinivasan K, Chen B, Alcamo E, McConell SK. 2008. The determination of projection neuron identity in the developing cerebral cortex. Curr Opin Neurobiol. 18:28–35.
Meyer G, Perez-Garcia CG, Gleeson JG. 2002. Selective expression of doublecortin and LIS1 in developing human cortex suggests unique modes of neuronal movement. Cereb Cortex. 12: 1225–1236.
Michele DE, Barresi R, Kanagawa M, Saito F, Cohn RD, Satz JS, Dollar J, Nishino I, Kelley RI, Somer H, et al. 2002. Post-translational disruption of dystroglycan-ligand interactions in congenital muscular dystrophies. Nature. 418:417–422.
Mochida GH, Walsh CA. 2004. Genetic basis of developmental malformations of the cerebral cortex. Arch Neurol. 61:637–640.
Molyneaux BJ, Arlotta P, Menezes JRL, Macklis JD. 2007. Neuronal subtype specification in the cerebral cortex. Nat Rev Neurosci. 8:427–437.
Nieto M, Monuki ES, Tang H, Imitola J, Haubst N, Khoury SJ, Cunningham J, Gotz M, Walsh CA. 2004. Expression of Cux-1 and Cux-2 in the subventricular zone and upper layers II-IV of the cerebral cortex. J Comp Neurol. 479:168–180.
Okazaki S, Ohsawa M, Kuki I, Kawawaki H, Koriyama T, Ri S, Ichiba H, Hai E, Inoue T, Nakamura H, et al. 2008. Aristaless-related homeobox gene disruption leads to abnormal distribution of GABAergic interneurons in human neocortex: evidence based on a case of X-linked lissencephaly with abnormal genitalia (XLAG). Acta Neuropathol. 116:453–462.
Olson EC, Walsh CA. 2002. Smooth, rough and upside-down neocortical development. Curr Opin Genet Dev. 12:320–327.
Rakic P. 2009. Evolution of the neocortex: a perspective from developmental biology. Nat Rev Neurosci. 10:724–735.
Reiner O, Sapir T. 2009. Polarity regulation in migrating neurons in the cortex. Mol Neurobiol. 40:1–14.
Sheen VL, Ferland RJ, Neal J, Harney M, Hill RS, Banham A, Brown P, Chenn A, Corbo J, Hecht J, et al. 2006. Neocortical neuronal arrangement in Miller Dieker syndrome. Acta Neuropathol. 111:489–496.
Simeone A, Acampora D, Mallamaci A, Stornaiuolo A, D'Apice MR, Nigro V, Boncinelli E. 1993. A vertebrate gene related to *orthodenticle* contains a homeodomain of the *bicoid* class and demarcates anterior neuroectoderm in the gastrulating mouse embryo. EMBO J. 12:2735–2747.
Spalice A, Parisi P, Nicita F, Pazzardi G, Del Balzo F, Iannetti. 2009. Neuronal migration disorders: clinical, neuroradiologic and genetic aspects. Acta Paediatr. 98:421–433.
Viot G, Sonigo P, Simon I, Simon-Bouy B, Chadeyron F, Beldjord C, Tantau J, Martinovic J, Esculpavit C, Brunelle F, et al. 2004. Neocortical neuronal arrangement in LIS1 and DCX lissencephaly may be different. Am J Med Genet A. 126A:123–128.
Weimann JM, Zhang YA, Levin ME, Devine WP, Brulet P, McConnell SK. 1999. Cortical neurons require otx1 for the refinement of exuberant axonal projections to subcortical targets. Neuron. 24:819–831.
Yamamoto T, Kato Y, Kawaguchi M, Shibata N, Kobayashi M. 2004. Expression and localization of fukutin, POMGnT1, and POMT1 in the central nervous system: consideration for functions of fukutin. Med Electron Microsc. 37:200–207.

THE JOURNAL OF BIOLOGICAL CHEMISTRY VOL. 287, NO. 17, pp. 13859–13867, April 20, 2012

Methyl CpG-binding Protein Isoform MeCP2_e2 Is Dispensable for Rett Syndrome Phenotypes but Essential for Embryo Viability and Placenta Development*[S]

Received for publication, October 2, 2011, and in revised form, February 26, 2012 Published, JBC Papers in Press, February 28, 2012, DOI 10.1074/jbc.M111.309864

Masayuki Itoh[‡1,2], **Candice G. T. Tahimic**[§1,3], **Shuhei Ide**[‡], **Akihiro Otsuki**[§], **Toshikuni Sasaoka**[¶], **Shigeru Noguchi**[‖4], **Mitsuo Oshimura**[§**], **Yu-ichi Goto**[‡], **and Akihiro Kurimasa**[§**]

*From the ‡Department of Mental Retardation and Birth Defect Research, National Institute of Neuroscience, National Center of Neurology and Psychiatry, Kodaira 187–8502, Japan, the §Institute of Regenerative Medicine and Biofunction, Graduate School of Medical Science, and the **21st Century Centers of Excellence Program, Research Core for Chromosome Engineering Technology, Tottori University, Yonago 683–8503, Japan, the ¶Department of Laboratory Animal Science, Kitasato University School of Medicine, Sagamihara 252–0374, Japan, and the ‖Signal Transduction Project, Kanagawa Academy of Science and Technology, Kawasaki 213–0012, Japan*

Background: There are two isoforms of *MeCP2*: *MeCP2_e1* and *_e2*. It is not known whether *MeCP2_e2* has specific functions *in vivo*.
Results: Deletion of *MeCP2_e2* results in no neurological phenotypes but confers a survival disadvantage to embryos and placenta defects.
Conclusion: *MeCP2_e2* functions in placenta development and embryo survival.
Significance: *MeCP2_e2* deletion results in a non-Rett syndrome phenotype but adversely affects embryo viability.

Methyl CpG-binding protein 2 gene (*MeCP2*) mutations are implicated in Rett syndrome (RTT), one of the common causes of female mental retardation. Two MeCP2 isoforms have been reported: *MeCP2_e2* (splicing of all four exons) and *MeCP2_e1* (alternative splicing of exons 1, 3, and 4). Their relative expression levels vary among tissues, with *MeCP2_e1* being more dominant in adult brain, whereas *MeCP2_e2* is expressed more abundantly in placenta, liver, and skeletal muscle. In this study, we performed specific disruption of the *MeCP2_e2*-defining exon 2 using the Cre-*loxP* system and examined the consequences of selective loss of MeCP2_e2 function *in vivo*. We performed behavior evaluation, gene expression analysis, using RT-PCR and real-time quantitative PCR, and histological analysis. We demonstrate that selective deletion of *MeCP2_e2* does not result in RTT-associated neurological phenotypes but confers a survival disadvantage to embryos carrying a *MeCP2_e2* null allele of maternal origin. In addition, we reveal a specific requirement for MeCP2_e2 function in extraembryonic tissue, where selective loss of MeCP2_e2 results in placenta defects and up-regulation of *peg-1*, as determined by the parental origin of the mutant allele. Taken together, our findings suggest a novel role for MeCP2 in normal placenta development and illustrate how paternal X chromosome inactivation in extraembryonic tissues confers a survival disadvantage for carriers of a mutant maternal *MeCP2_e2* allele. Moreover, our findings provide an explanation for the absence of reports on *MeCP2_e2*-specific exon 2 mutations in RTT. *MeCP2_e2* mutations in humans may result in a phenotype that evades a diagnosis of RTT.

Methyl CpG-binding protein 2 gene (*MeCP2*) mutations are implicated in Rett syndrome (RTT),[5] one of the common causes of female mental retardation (1, 2). RTT patients exhibit apparently normal early psychomotor development and then gradually lose previously acquired psychomotor skills. Stereotypic hand movements and microcephaly are also clinical features of this disorder (3). MeCP2 binds to methylated CpG dinucleotides and functions as a transcriptional repressor through its interactions with the Sin3A/histone deacetylase complex and the SWI/SNF chromatin remodeling complex (4–8). To date, two MeCP2 isoforms have been characterized. The first reported MeCP2 isoform, referred to as MeCP2_e2 (translational start site in exon 2; also known as MeCP2A or MeCP2β), is generated by splicing of all four exons and has a translation start site in the middle of exon 2. The more recently discovered isoform, MeCP2_e1 (translational start site in exon 1; also known as MeCP2B or MeCP2α), results from alternative splicing of exons 1, 3, and 4 and has a translation start site in exon 1 (9, 10). Their relative expression levels vary among tissues, with MeCP2_e1 being more dominant in adult brain, whereas MeCP2_e2 is expressed more abundantly in placenta,

* This work was supported by Ministries of Health, Labor, and Welfare Grants 15B-3, 18A-3, H21-Nanchi-Ippan-110, and H22-Nanchi-Ippan-133 and by Ministries of Education, Culture, Science, Sports, and Technology of Japan Grant 18390304.
[S] This article contains supplemental Fig. 1.
[1] Both authors contributed equally to this work.
[2] To whom correspondence should be addressed: 4-1-1 Ogawahigashi, Kodaira, Tokyo 187-8502, Japan. Tel.: 81-423461713; Fax: 81-423461743; E-mail: itoh@ncnp.go.jp.
[3] Recipient of a Japanese Government Research Scholarship. Present address: Endocrine Unit, San Francisco Veterans Affairs Medical Center, San Francisco, CA 94121.
[4] Present address: Pharmaceuticals Analysis Group, Food Analysis and Safety Assessment Center, Food Technology Research Laboratories, R&D Division, Meiji Co. Ltd., Odawara 250–0862, Japan.

[5] The abbreviations used are: RTT, Rett syndrome; TRE, tetracycline-responsive promoter; tTA, tetracycline transactivator; XCI, X chromosome inactivation; PGK, phosphoglycerate kinase.

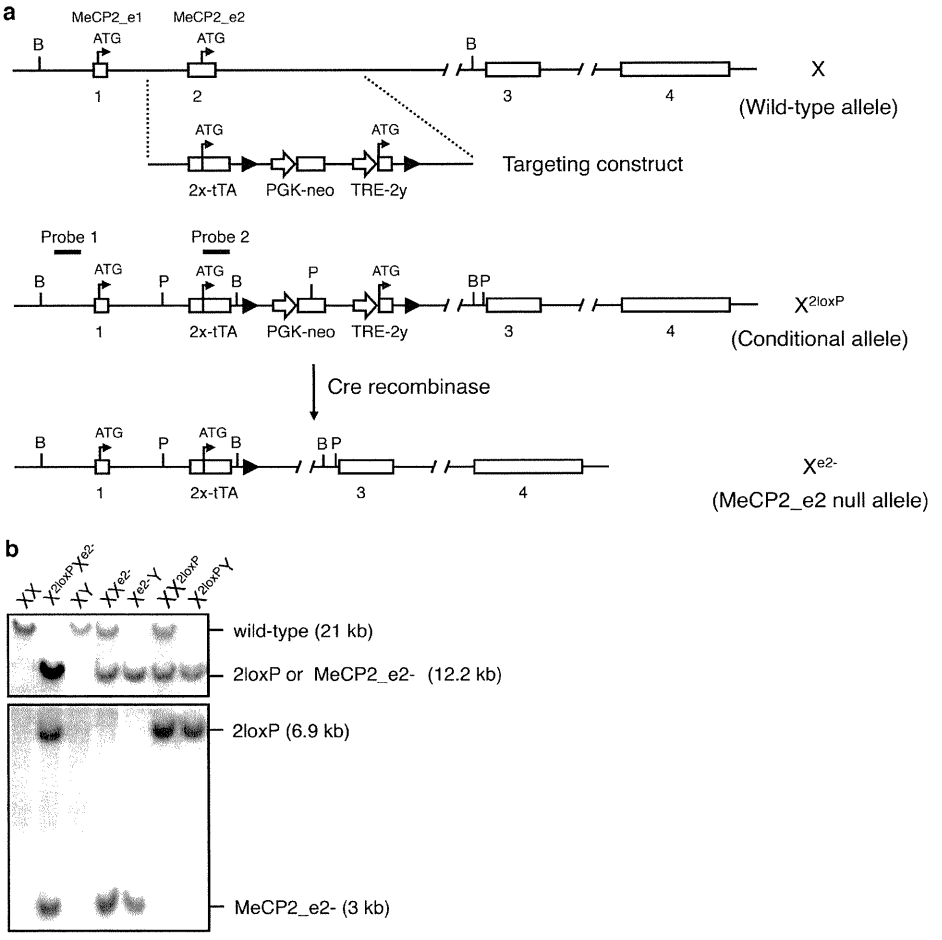

FIGURE 1. **Generation of *MeCP2_e2*-deficient mice.** *a*, strategy for selective targeting of *MeCP2_e2*. Transcription start sites for *MeCP2_e2* and *MeCP2_e1* before and after exon 2 disruption are shown. *loxP* sites are denoted as *filled triangles*. Relative location of probes for Southern hybridization, and positions of restriction enzymes BamHI (*B*) and PvuII (*P*) are indicated. Crossing of *MeCP2_e2* conditional mice with Nestin-Cre deleter mice results in the excision of the transcriptional start site of *MeCP2_e2* and the creation of the *MeCP2_e2* null allele, not only in neuronal cells but also in the germ line. Note that the transcriptional start of *MeCP2_e1* remains intact after disruption of the *MeCP2* locus. *b*, *MeCP2_e2* wild-type and mutant alleles as differentiated by two sets of Southern hybridization. For the first screening (*top*), genomic DNA was digested with BamHI and probed to visualize the presence of the targeted MeCP2 locus containing the exon 2x-tTA sequence. In the second screening (*bottom*), PvuI-digested genomic DNA was probed to differentiate between the conditional (X^{2loxP}) and null (X^{e2-}) alleles. Approximate band sizes are indicated in parentheses.

liver, and skeletal muscle (10). The most common MeCP2 mutations in RTT occur in exons shared by both isoforms (11). However, no mutation in the *MeCP2_e2*-defining exon 2 has ever been reported in RTT. In this study, we performed specific disruption of the *MeCP2_e2*-defining exon 2 using the Cre-*loxP* system and examined the consequences of selective loss of MeCP2_e2 function *in vivo*.

EXPERIMENTAL PROCEDURES

Selective Targeting of MeCP2_e2—The *MeCP2_e2* null allele was generated by Cre recombinase-mediated excision of exon 2 in *MeCP2_e2* conditional mice (Fig. 1). MeCP2 sequences were either directly derived or amplified from genomic DNA obtained from CJ7 ES cells or a BAC clone carrying the MeCP2 locus. The 5′-end of the targeting vector consisted of a 1.2-kb region possessing homology to intron 1 and was generated by high fidelity PCR. The early part of exon 2 containing the untranslated region (referred to as exon 2x) was fused to the tetracycline transactivator (tTA) gene, having a stop codon and poly(A) sequence. The latter half of exon 2 (referred to as exon 2y) beginning from the ATG start site of MeCP2_e2 was placed under the control of the tetracycline-responsive promoter, TRE. A pair of *loxP* sites flanked this TRE-exon 2y sequence. A PGK-driven neomycin selection marker was positioned between the first *loxP* site and the TRE-2y region. The 3′ arm of the targeting vector consisted of a 5.9-kb EcoRI fragment derived from intron 2.

Generation of MeCP2_e2 Null Mice—A correctly targeted ES cell clone, confirmed by Southern blot analysis, was injected into 3.5-day postconception (dpc) C57BL/6J blastocysts. Approximately 10 ES cells were injected per blastocyst, and 20 blastocysts were transferred to each pseudopregnant recipient. The resulting chimeric offspring were intercrossed mice to generate F1 progeny. For deletion of MeCP2_e2, we crossed MeCP2_e2$^{+/2loxP}$ females with deleter mice carrying a Cre recombinase transgene under the control of the Nestin promoter. However, leaky expression from Nestin promoter-driven Cre recombinase induced a deletion in the germ line, resulting in progeny that carried the *MeCP2_e2* null allele

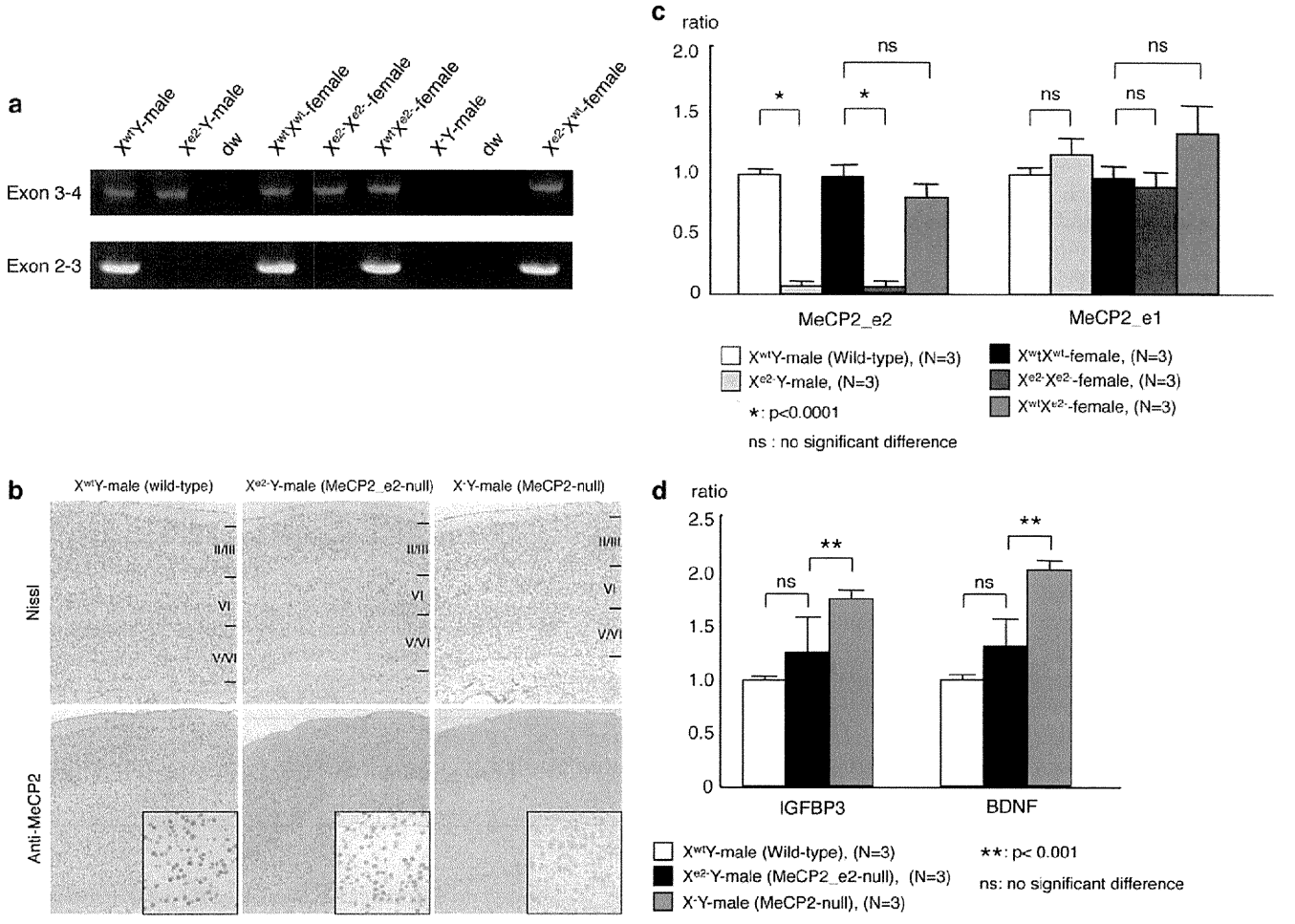

FIGURE 2. **Absence of RTT-associated phenotypes in *MeCP2_e2*-deficient mice.** *a*, reverse transcription PCR showing the selective loss of *MeCP2_e2* transcripts in brains of *MeCP2_e2* null males and females at P28. *b*, sections of P28 mouse brain were stained with cresyl violet to visualize neurons. Immunochemical staining was performed using anti-MeCP2 antibody. The *MeCP2*-deficient mouse, a previously reported *MeCP2_e2* and *MeCP2_e1* knockout (12), shows thinning of the cerebral cortex and no MeCP2-immunopositive cells. *MeCP2_e2* null mouse exhibits MeCP2-immunopositive cells in the cerebral cortex. *c*, real-time PCR analysis of *MeCP2_e2* and *MeCP2_e1* of P28 brains. The *MeCP2_e2*-deficient mouse shows *MeCP2_e1* expression but not *MeCP2_e2*, as indicated by the presence of exons 3 and 4 and the absence exons 2 and 3. *d*, quantitation of BDNF and IGFBP3 transcripts in P0 *MeCP2_e2*-deficient mice by real-time PCR. An $X^{wt}Y$ male mouse was used as a reference. Statistical analysis was performed using Student's *t* test at $p < 0.0001$ (*) and $p < 0.001$ (**). *Error bars*, S.D.

TABLE 1

Offspring distribution at 4 weeks of age; crossing of $X^{wt}X^{e2-}$ females and $X^{wt}Y$ males (maternal transmission of MeCP2_e2 null allele)

χ sum = 107.04, $p < 0.0001$. % Change = (% observed value − % expected value)/% expected value) × 100.

	$X^{wt}X^{wt}$	$X^{e2-}X^{wt}$	$X^{wt}Y$	$X^{e2-}Y$	Total
Observed	52 (27%)	27 (14%)	101 (53%)	12 (6%)	192
Estimated	48 (25%)	48 (25%)	48 (25%)	48 (25%)	192
% Change	8%	−44%	−112%	−76%	

TABLE 2

Offspring distribution at 4 weeks of age; crossing of $X^{wt}X^{e2-}$ females and $X^{e2-}Y$ males (biparental transmission of MeCP2_e2 null allele)

χ sum = 16.20, $p < 0.002$. % Change = (% observed value − % expected value)/% expected value) × 100.

	$X^{wt}X^{e2-}$	$X^{e2-}X^{e2-}$	$X^{wt}Y$	$X^{e2-}Y$	Total
Observed	11 (28%)	4 (10%)	20 (50%)	5 (12%)	40
Estimated	10 (25%)	10 (25%)	10 (25%)	10 (25%)	40
% Change	10%	−60%	100%	−50%	

(X^{e2-}). This population was expanded and used in succeeding experiments. Genotypes of the resulting progeny were assessed by an initial PCR screen followed by two sets of Southern blotting. The *MeCP2_e2* null allele was generated by Cre recombinase-mediated excision of exon 2 in *MeCP2_e2* conditional mice (Fig. 1). A previously reported MeCP2 null mouse, B6.129P2(C)-*Mecp2*$^{tm1.1Bird}$ (described as $MeCP2^{-/y}$), generated by targeted disruption of exons 3 and 4 (12), was obtained from Jackson Laboratory (Bar Harbor, ME) and used as a control for some of the experiments. All animal studies were performed with the approval of the Animal Care Committee of the National Institute of Neuroscience, National Center of Neurology and Psychiatry, Japan.

RT-PCR and Real-time Quantitative PCR—We prepared 3–8 fresh frozen brains and placentas of various genotypes at 13.5 dpc and postnatal days 0 (P0) and 28 (P28). Total RNA was isolated from mouse tissue using the RNeasy minikit (Qiagen, Valencia, CA) following the manufacturer's recommendations. We carried out reverse transcription with the First-Strand cDNA synthesis kit (Amersham Biosciences) or TaqMan

reverse transcription reagents (Applied Biosystems, Foster City, CA) using oligo(dT). Primer sequences and annealing conditions are as follows: for MECP2 exons 2 and 3, 5′-TTAGGGCTCAGGGAGGAAAA-3′ (forward) and 5′-CAAAATCATTAGGGTCCAAGG-3′ (reverse) with annealing temperature of 50 °C and expected PCR product size of 451 bp; for *MECP2* exons 3 and 4, 5′-ATTATCCGTGACCGGGGA-3′ (forward) and 5′-TGATGCTGCTGCCTTTGGT-3′ (reverse) with annealing temperature of 55 °C and an expected PCR product size of 354 bp.

For quantitative analysis, we carried out PCR amplifications using Universal PCR Master Mix (Applied Biosystems) according to the manufacturer's recommendations in a real-time ABI PRISM 7700 platform (Applied Biosystems). Relative transcript ratios were normalized to GAPDH RNA. Primers and probes for mouse *MeCP2* (common sequence of *MeCP2_e2* and *MeCP2_e1*), *MeCP2_e2*, *MAP2*, *IGFBP3*, and *BDNF* are available from Applied Biosystems. The probes 5′-CGCCGAGCGGAGGAG-3′ and 5′-CCTGGTCTTCTGACTTTTCTTCCA were designed to amplify a portion of the *MeCP2_e1* transcript, and a probe of CCTCCTCGCCTCCTCC-3′ was used. Sequence Detection System 1.7 software (Applied Biosystems) was used for analysis.

Immunohistochemical Analysis and TUNEL Assay—Tissues were fixed in 4% paraformaldehyde and then embedded in paraffin. Three-micrometer sections were prepared and stained with cresyl violet to visualize neurons. Purified MeCP2 antibody (provided by Dr. S. Kudo, Hokkaido Institute of Public Health, Sapporo, Japan), cleaved caspase-3 antibody (Chemicon International Inc., Temecula, CA), Peg-1 antibody (Atlas Antibodies AB, Stockholm, Sweden), and CRCX4 antibody (Abnova, Taipei, Taiwan) were used for immunohistological experiments. TUNEL assays were performed using terminal deoxynucleotidyltransferase (Roche Applied Science) following the manufacturer's recommendations.

Behavior Analysis—We performed tail suspension, footprinting, and open field analysis, using 4- or 5-week-old wild-type, MeCP2_e2^{-}, MeCP2_e2^{2loxP}, and MeCP2$^{-/y}$ males.

Statistical Analysis—Statistical analysis was performed using the χ^2 test. Animal crossings were performed to evaluate the effect of parent-specific transmission of the MeCP2_e2 null allele using appropriate sample sizes. Statistical significance of the expression levels was evaluated using Student's *t* test with a significance level of $p < 0.05$.

RESULTS AND DISCUSSION

MeCP2_e2-null Mouse Generation—We generated the *MeCP2_e2* mutant allele (X^{e2-}) by crossing mice carrying a tetracycline-inducible *MeCP2_e2* conditional allele (X^{2loxP}) with deleter mice carrying a Nestin-driven Cre recombinase transgene (Fig. 1). We observed germ line transmission of the *MeCP2_e2* null allele in some of the F3 generation (Fig. 1), probably resulting from leaky expression of Nestin-driven Cre recombinase in non-brain tissue. This subpopulation was expanded, and the F10 to F12 generations were used for the experiments in this study. We confirmed loss of MeCP2_e2 expression, whereas *MeCP2_e1* transcription remained intact in these animals (Fig. 2, *a* and *c*). Brain histological analysis showed no difference between *MeCP2_e2* null mouse and wild-type mice (Fig. 2*b*).

TABLE 3

Offspring distribution at 4 weeks of age; crossing of $X^{wt}X^{wt}$ females and $X^{e2-}Y$ males (paternal transmission of MeCP2_e2 null allele)

χ sum = 2.28, no significant difference. % Change = (% observed value − % expected value)/% expected value) × 100.

	$X^{wt}X^{e2-}$	$X^{wt}Y$	Total
Observed	50 (48%)	55 (52%)	105
Estimated	52.5 (50%)	52.5 (50%)	105
% Change	−4%	4%	

TABLE 4

Offspring distribution at 13.5 dpc; crossing of $X^{wt}X^{e2-}$ females and $X^{wt}Y$ males (maternal transmission of MeCP2_e2 null allele)

χ sum = 13.25, $p < 0.005$. % Change = (% observed value − % expected value)/% expected value) × 100.

	$X^{wt}X^{wt}$	$X^{e2-}X^{wt}$	$X^{wt}Y$	$X^{e2-}Y$	Total
Observed	36 (28%)	28 (22%)	46 (36%)	18 (14%)	128
Estimated	32 (25%)	32 (25%)	32 (25%)	32 (25%)	128
% Change	13%	−13%	44%	−44%	

TABLE 5

Offspring distribution at 13.5 dpc; crossing of $X^{wt}X^{wt}$ females and $X^{e2-}Y$ males (paternal transmission of MeCP2_e2 null allele)

χ sum = 2.28, no significant difference. % Change = (% observed value − % expected value)/% expected value) × 100.

	$X^{wt}X^{e2-}$	$X^{wt}Y$	Total
Observed	27 (61%)	17 (39%)	44
Estimated	22 (50%)	22 (50%)	44
% Change	23%	−23%	

Phenotypes and Expression Analyses of MeCP2_e2-null Mice—At birth, mice carrying *MeCP2_e2* mutant alleles were indistinguishable from wild-type littermates. They developed into fertile adults and did not display any neurological deficits observed in murine models for RTT (12, 13), indicating that MeCP2_e1 is sufficient to carry on the functions of MeCP2 in the brain. Moreover, mice carrying MeCP2_e2 mutant alleles lived as long as their wild-type siblings, over 2 years (data not shown). Immunohistochemical staining of brain tissue from $X^{e2-}Y$ and $X^{wt}X^{e2-}$ animals at 28 days of age revealed normal morphology of neuronal layers in contrast to the denser packaging of neurons in a previously reported RTT model wherein both MeCP2 isoforms have been knocked out (Fig. 2*b*) (14, 15). Taken together, these results demonstrate that loss of MeCP2_e1 function is not sufficient to cause RTT-associated neurological phenotypes.

To examine the implications of *MeCP2_e2* deficiency on MeCP2 transcriptional silencing activity, we checked mRNA levels of two MeCP2-regulated genes, insulin like growth factor binding protein 3 (*IGFBP3*) (16, 17) and brain-derived nerve growth factor (*BDNF*) (18). The mRNA levels of these genes in brains of $X^{e2-}Y$ mice did not significantly differ from those of age-matched wild-type males (Fig. 2*d*). In contrast, IGFBP3 and BDNF transcript levels increased by 1.6- and 2-fold, respectively, in the $X^{-}Y$ total MeCP2 knockout. These findings indi-

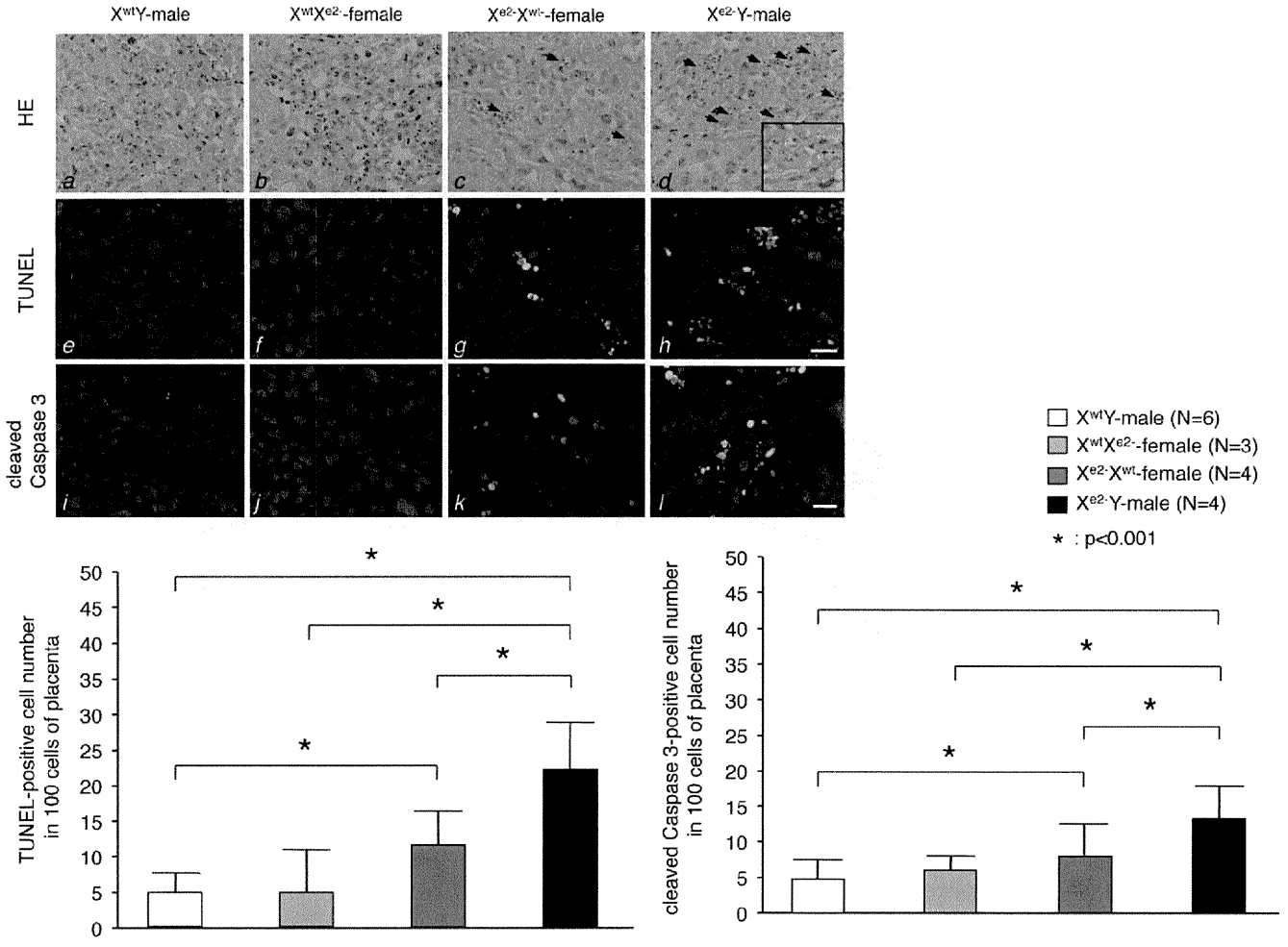

FIGURE 3. ***MeCP2_e2* deficiency results in placenta abnormalities.** The *top panels* (*a–d*) show placenta sections stained with hematoxylin and eosin. The *inset* shows the section at higher magnification. *Arrows* show apoptotic cells. The *middle panels* (*e–h*) show TUNEL staining of the same sections. Apoptotic nuclei appear as multiple spots (*yellow*), indicating DNA fragmentation. Propidium iodide was used as counterstain. The *bottom panels* (*i–l*) show cleaved caspase-3 immunostaining of the placenta. TUNEL-positive cells are indicated by *arrows*. *Scale bar*, 25 μm. An increase in the number of TUNEL-positive cells and cleaved caspase 3-positive cells was observed in the placentas of $X^{e2-}X^{wt}$ and $X^{e2-}Y$ embryos having a maternal *MeCP2_e2* null allele (refer to *bar graphs* in *lower panel* for quantitation) *, $p < 0.001$; *brackets* and *asterisks* indicate significant differences. *Error bars*, S.D.

cate that MeCP2_e2 is not essential for mediating transcriptional silencing of MeCP2 target genes in the brain.

Parent-specific Effects of MeCP2_e2 Null Allele Birth Rates—We next examined whether *MeCP2_e2* deficiency mediated any other non-neuronal phenotype. Interestingly, we observed reduced births of progeny that carried *MeCP2_e2* null allele of maternal origin. Specifically, we found a 76% reduction in $X^{e2-}Y$ males and a 44% reduction in $X^{e2-}X^{wt}$ females born to $X^{wt}X^{e2-}$ female and wild-type male pairings (Table 1). Similarly, in $X^{e2-}X^{wt}$ and $X^{e2-}Y$ pairings, $X^{e2-}Y$ and $X^{e2-}X^{e2-}$ births were reduced by 50 and 60%, respectively (Table 2). In contrast, birth rates of $X^{wt}X^{e2-}$ females (having a paternal X^{e2-}) did not deviate from the expected values (Tables 2 and 3). We exclude the possibility that these were nonspecific effects resulting from toxicity of the tTA in the targeting vector because no such decreases in births were observed in an unrelated transgenic mouse model carrying the same vector backbone.[6] Taken together, these results point to an association between reduced embryo viability and a maternally transmitted *MeCP2_e2* null allele.

To further delineate the time period at which selection against embryos carrying maternal *MeCP2_e2* null alleles occurred, we examined the genotype distribution at 13.5 dpc and observed similar trends (Tables 4 and 5). Moreover, we did not find any evidence of resorbed embryos at this time point (data not shown). We also performed morphological assessment of the uterus at preimplantation and postimplantation stages and found no abnormalities in preimplantation sites and the implantation process (data not shown). Nevertheless, these findings suggest that the reduced number of embryos carrying a mutant maternal *MeCP2_e2* allele is due neither to a failure in implantation nor to embryo lethality at postimplantation but to reduced viability of the embryo prior to implantation or early embryonic lethality after implantation.

Maternally Transmitted MeCP2_e2 Null Allele Results in Apoptosis and Altered peg-1 Expression in Placenta—During early development of the female mammal, one of the two X chromosomes becomes transcriptionally inactive to allow dos-

[6] A. Otsuki and A. Kurimasa, unpublished results.

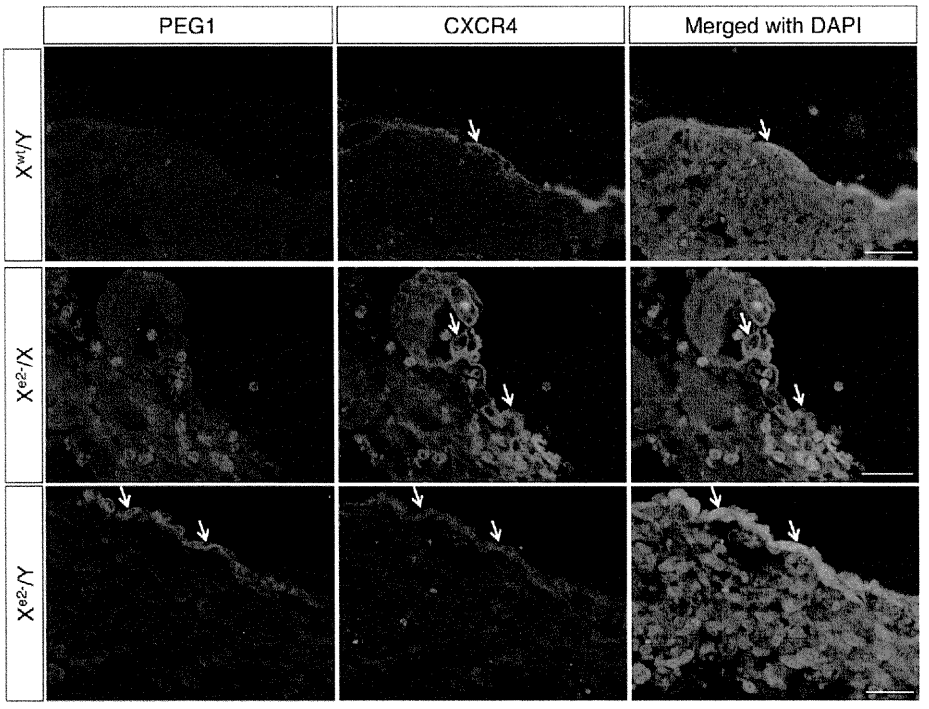

FIGURE 4. **Loss of maternal MeCP2_e2 results in failure to silence *peg-1* expression in trophoblast cells.** CXCR4 is a trophoblast cell marker. X^{wt}/Y and $X^{e2-}X^{wt}$ placenta have minimal *peg-1* expression, whereas X^{e2-}/Y placenta show elevated *peg-1* levels in trophoblast cells (*arrows*). *Scale bars*, 50 μm.

age compensation of X-linked genes (19, 20). In mouse extraembryonic lineages, such as placenta, the paternally derived X chromosome undergoes preferential inactivation, a phenomenon called imprinted paternal X chromosome inactivation (XCI) (21, 22). Hence, we examined the effect of *MeCP2_e2* deficiency in placenta tissue at 13.5 dpc. Interestingly, placentas of embryos carrying a maternal *MeCP2_e2* null allele exhibited increased apoptosis, which was more notable in placentas of males (Fig. 3). These TUNEL-positive cells expressed peg-1 (supplemental Fig. 1), an imprinted gene known to function in placenta development (23, 24). In contrast, very few apoptotic cells were observed in the placenta of $X^{wt}X^{e2-}$ embryos carrying a paternal *MeCP2_e2* null allele (Fig. 3). In addition, immunostaining revealed increased Peg-1 levels in cells expressing CXCR4, a trophoblast marker (25), in the placenta of animals carrying a maternal *MeCP2_e2* null allele (Fig. 4 and supplemental Fig. 1). Taken together, our results indicate that MeCP2_e2 is essential for the maintenance of *peg-1* silencing in trophoblast cells and that elevated expression of *peg-1* in the placenta has deleterious effects on cell survival.

We also examined transcript levels of *peg-1* and other imprinted genes involved in placenta function, such as *peg-3*, *igf-2*, and *h19* (23). Among these four genes, *peg-1* exhibited elevated transcript levels in the placenta of embryos carrying a maternal mutant allele (Fig. 5*a*), in concordance with our immunohistological findings. The mRNA levels of the other three genes were unchanged (Fig. 5*a*). In placentas of animals carrying the *MeCP2* two-isoform knock-out allele, *peg-1* expression was also elevated (Fig. 5*b*). The *peg-1* transcript levels were not due to deregulation of imprinting in placenta because imprinted paternal XCI was found to be intact in these animals (Fig. 5*c*). Rather, elevated *peg-1* transcript levels directly correlate with the loss of *MeCP2_e2* expression effected by imprinted paternal XCI. These findings indicate that *MeCP2_e2*-specific transcriptional silencing activity is essential for the regulation of *peg-1* expression and possibly of other genes in placenta.

The imprinted gene *peg-1*, located in murine chromosome 6, has been reported to play a role in angiogenesis in extraembryonic tissue (26). Mutations in *peg-1* have also been implicated in placenta failure (24, 25) and embryonic growth retardation (27). One group has reported that paternally expressed transcripts are associated with premature placenta (28). Interestingly, paternal transmission of a *peg-1* null allele in heterozygous mice results in diminished postnatal survival rates, whereas maternal transmission does not generate any remarkable phenotype (27, 29). It is clear from these reports that deregulation of *peg-1* expression or imprinting status has deleterious consequences on embryo viability and placenta function. Our current study demonstrates that MeCP2_e2 is an essential regulator of *peg-1* expression in extraembryonic tissue. As for how increased *peg-1* expression correlates with observed placenta defects in carriers of a maternal *MeCP2_e2* null allele, we propose a scenario wherein perturbations in *peg-1* expression results in disruption of biological pathways that involve Peg-1, leading to enhanced apoptosis in placenta. Peg-1 is a membrane-bound protein that is predicted to have lipase or acyltransferase activity based on sequence homology with the α/β-hydrolase superfamily of proteins (30). Lipid metabolism is a very important biological process and is critical for the developing embryo and placenta. We propose that loss of *MeCP2_e2* results in failure to transcriptionally silence *peg-1* in extraem-

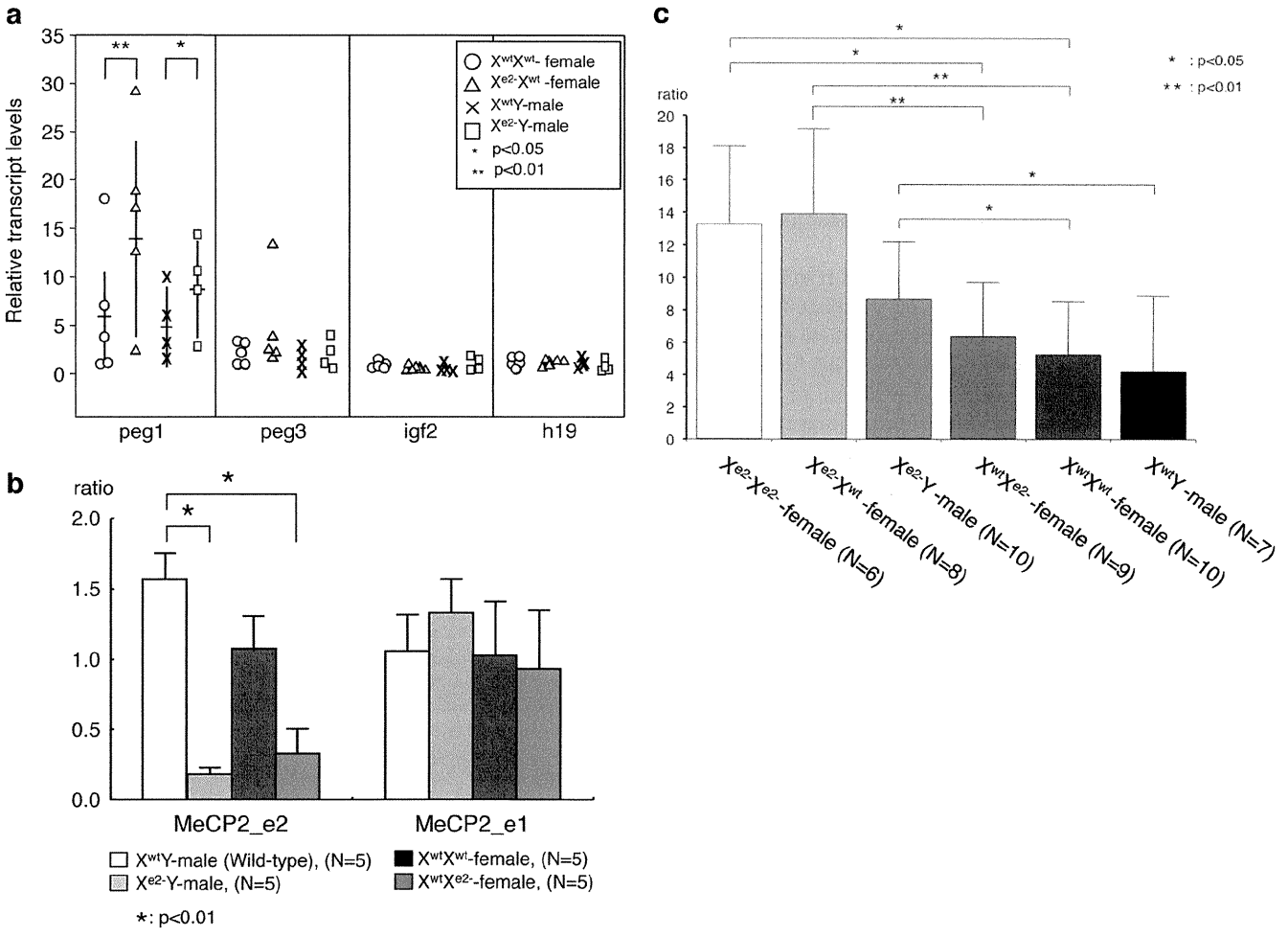

FIGURE 5. **Quantitative PCR analysis of placenta.** Shown are (*a*) placenta transcript levels of selected imprinted genes, *peg-1*, *peg-3*, *igf-2*, and *h19*, from 13.5 dpc embryos and (*b*) placenta transcript levels of peg-1 in *MeCP2_e2* and *MeCP2_e1* (two-isoform knockout) mutants. The *horizontal* and *vertical bars* of *peg-1* transcripts (*a*) show averages and S.D. of each genotype, respectively. *c*, *peg-1* expression in placentas of various genotypes. Maternally derived X^{e2-} allele up-regulated *peg-1* expression. *, $p < 0.05$; **, $p < 0.001$. *Brackets* and *asterisks* indicate significant differences. *Error bars*, S.D.

bryonic tissue, leading to increased Peg-1 enzymatic activity, aberrant regulation of Peg-1 binding partners or downstream targets, and, ultimately, apoptosis.

We have earlier stated that we found the implantation process to be normal for these animals. Moreover, at 13.5 dpc, there was no evidence of resorbed embryos, and the skewed embryo genotypes resembled that from postnatal analysis. These results, taken together with the increased number of apoptotic trophoblast cells and elevated *peg-1* expression in embryos carrying a maternal *MeCP2_e2* null allele, suggest that the loss of *MeCP2_e2* leads to trophoblast dysfunction during preimplantation through abnormal *peg-1* expression. Furthermore, we view the increase in apoptotic trophoblast cells as a persisting phenotype brought about by early perturbation of placenta gene expression. In mice, placental development begins in the blastocyst at embryonic day 3.5 when the trophectoderm layer becomes distinct from the inner cell mass (32). The trophoblast that lines the blastocyst plays an important role during attachment to the endometrium and in the formation of the placenta (31, 32). It has been reported by other groups that trophoblast dysfunction leads to disruption of placenta formation and reduction of birth number (31, 33). In our current study, we have shown that loss of *MeCP2_e2* results in a trophoblast defect that ultimately leads to reduced embryo viability.

Because some carriers of a mutant *MeCP2_e2* allele are born and develop into healthy adults, we hypothesize that the placenta abnormalities in these animals may have been overcome by *de novo MeCP2_e1* compensation or some other adaptation. In some types of extraembryonic cells, XCI can follow either a paternal or maternal pattern (34, 35). In somatic tissue, relaxation of imprinting occurs in certain pathological conditions (28, 36), and epigenetic heterogeneity at imprinted loci of autosomal chromosomes influences individual traits (37). The absence of *MeCP2_e2* correlated with up-regulation of *peg-1* expression, indicating a disturbance in regulation of downstream *MeCP2* gene targets. Although increased apoptosis in placenta could be used to explain the decreased viability of $X^{e2-}Y$ mice, this may also be interpreted as a way to eliminate functionally defective cells, thus contributing to the survival of some embryos.

The deleterious effects of *MeCP2* mutations have been viewed mostly in the context of somatic XCI patterns. A num-

ber of studies have addressed the contribution of XCI to the pathogenesis of *MeCP2* mutations (38, 39). It is suggested that XCI patterns may partly explain phenotypic variability in human RTT with *MeCP2* mutations (38) and in mouse RTT models (39). Our findings indicate that this is not the full picture and that paternal X chromosome inactivation in the extraembryonic lineage also contributes to the deleterious consequences of *MeCP2* mutations and, most likely, other X-linked gene mutations.

Recently, it has been reported that transgenic expression of either the *MeCP2_e1* or *MeCP2_e2* splice variant prevents the development of RTT-like neuronal phenotypic manifestations in a mouse model lacking *MeCP2*. This finding indicates that either *MeCP2* splice variant is sufficient to fulfill MeCP2 function in the mouse brain (40). Our findings reveal a novel mechanism for the pathogenesis of *MeCP2* mutations in extraembryonic tissue, wherein maternally inherited *MeCP2_e2* mutations result in placenta abnormalities that ultimately lead to a survival disadvantage for carriers of this mutant allele. Our study also provides an explanation for the absence of reports on *MeCP2_e2*-specific exon 2 mutations in RTT. It is conceivable that *MeCP2_e2* mutations in humans may result in a phenotype that evades a diagnosis of RTT. Moreover, the possible link between a novel genetic disorder characterized by reduced embryo viability and MeCP2 exon 2 mutations is a concept that merits further exploration. In summary, we have demonstrated that MeCP2_e2 is dispensable for RTT-associated neurological phenotypes. We have also discovered a novel requirement for MeCP2_e2 in placenta and embryo viability and have provided proof of existence of isoform-specific functions for two MeCP2 splicing variants.

Acknowledgments—We thank Dr. S. Kudo for the MeCP2 antibody and helpful suggestions and S. Kumagai and N. Tomimatsu for help with some of the experiments.

REFERENCES

1. Amir, R. E., Van den Veyver, I. B., Wan, M., Tran, C. Q., Francke, U., and Zoghbi, H. Y. (1999) Rett syndrome is caused by mutations in X-linked MECP2, encoding methyl-CpG-binding protein 2. *Nat. Genet.* **23,** 185–188
2. Rett, A. (1966) [On an unusual brain atrophy syndrome in hyperammonemia in childhood]. *Wien Med. Wochenschr.* **116,** 723–726
3. Hagberg, B., Aicardi, J., Dias, K., and Ramos, O. (1983) A progressive syndrome of autism, dementia, ataxia, and loss of purposeful hand use in girls. Rett's syndrome. Report of 35 cases. *Ann. Neurol.* **14,** 471–479
4. Lewis, J. D., Meehan, R. R., Henzel, W. J., Maurer-Fogy, I., Jeppesen, P., Klein, F., and Bird, A. (1992) Purification, sequence, and cellular localization of a novel chromosomal protein that binds to methylated DNA. *Cell* **69,** 905–914
5. Meehan, R. R., Lewis, J. D., and Bird, A. P. (1992) Characterization of MeCP2, a vertebrate DNA-binding protein with affinity for methylated DNA. *Nucleic Acids Res.* **20,** 5085–5092
6. Nan, X., Ng, H. H., Johnson, C. A., Laherty, C. D., Turner, B. M., Eisenman, R. N., and Bird, A. (1998) Transcriptional repression by the methyl-CpG-binding protein MeCP2 involves a histone deacetylase complex. *Nature* **393,** 386–389
7. Jones, P. L., Veenstra, G. J., Wade, P. A., Vermaak, D., Kass, S. U., Landsberger, N., Strouboulis, J., and Wolffe, A.P. (1998) Methylated DNA and MeCP2 recruit histone deacetylase to repress transcription. *Nat. Genet.* **2,** 187–191
8. Harikrishnan, K. N., Chow, M. Z., Baker, E. K., Pal, S., Bassal, S., Brasacchio, D., Wang, L., Craig, J. M., Jones, P. L., Sif, S., and El-Osta, A. (2005) Brahma links the SWI/SNF chromatin-remodeling complex with MeCP2-dependent transcriptional silencing. *Nat. Genet.* **37,** 254–264
9. Kriaucionis, S., and Bird, A. (2004) The major form of MeCP2 has a novel N terminus generated by alternative splicing. *Nucleic Acids Res.* **32,** 1818–1823
10. Mnatzakanian, G. N., Lohi, H., Munteanu, I., Alfred, S. E., Yamada, T., MacLeod, P. J., Jones, J. R., Scherer, S. W., Schanen, N. C., Friez, M. J., Vincent, J. B., and Minassian, B. A. (2004) A previously unidentified MECP2 open reading frame defines a new protein isoform relevant to Rett syndrome. *Nat. Genet.* **36,** 339–341
11. Bienvenu, T., and Chelly, J. (2006) Molecular genetics of Rett syndrome. When DNA methylation goes unrecognized. *Nat. Rev. Genet.* **7,** 415–426
12. Guy, J., Hendrich, B., Holmes, M., Martin, J. E., and Bird, A. (2001) A mouse Mecp2-null mutation causes neurological symptoms that mimic Rett syndrome. *Nat. Genet.* **27,** 322–326
13. Chen, R. Z., Akbarian, S., Tudor, M., and Jaenisch, R. (2001) Deficiency of methyl-CpG binding protein-2 in CNS neurons results in a Rett-like phenotype in mice. *Nat. Genet.* **27,** 327–331
14. Fukuda, T., Itoh, M., Ichikawa, T., Washiyama, K., and Goto, Y. (2005) Delayed maturation of neuronal architecture and synaptogenesis in cerebral cortex of Mecp2-deficient mice. *J. Neuropathol. Exp. Neurol.* **64,** 537–544
15. Dragich, J. M., Kim, Y. H., Arnold, A. P., and Schanen, N. C. (2007) Differential distribution of the MeCP2 splice variants in the postnatal mouse brain. *J. Comp. Neurol.* **501,** 526–542
16. Chang, Y. S., Wang, L., Suh, Y. A., Mao, L., Karpen, S. J., Khuri, F. R., Hong, W. K., and Lee, H. Y. (2004) Mechanisms underlying lack of insulin-like growth factor-binding protein-3 expression in non-small-cell lung cancer. *Oncogene* **23,** 6569–6580
17. Itoh, M., Ide, S., Takashima, S., Kudo, S., Nomura, Y., Segawa, M., Kubota, T., Mori, H., Tanaka, S., Horie, H., Tanabe, Y., and Goto, Y. (2007) Methyl CpG-binding protein 2 (a mutation of which causes Rett syndrome) directly regulates insulin-like growth factor binding protein 3 in mouse and human brains. *J. Neuropathol. Exp. Neurol.* **66,** 117–123
18. Chen, W. G., Chang, Q., Lin, Y., Meissner, A., West, A. E., Griffith, E. C., Jaenisch, R., and Greenberg, M. E. (2003) Derepression of BDNF transcription involves calcium-dependent phosphorylation of MeCP2. *Science* **302,** 885–889
19. Mak, W., Nesterova, T. B., de Napoles, M., Appanah, R., Yamanaka, S., Otte, A. P., and Brockdorff, N. (2004) Reactivation of the paternal X chromosome in early mouse embryos. *Science* **303,** 666–669
20. Sado, T., and Ferguson-Smith, A. C. (2005) Imprinted X inactivation and reprogramming in the preimplantation mouse embryo. *Hum. Mol. Genet.* **14,** R59–64
21. Takagi, N., and Sasaki, M. (1975) Preferential inactivation of the paternally derived X chromosome in the extraembryonic membranes of the mouse. *Nature* **256,** 640–642
22. Harper, M. I., Fosten, M., and Monk, M. (1982) Preferential paternal X inactivation in extraembryonic tissues of early mouse embryos. *J. Embryol. Exp. Morphol.* **67,** 127–135
23. Obata, Y., Kaneko-Ishino, T., Koide, T., Takai, Y., Ueda, T., Domeki, I., Shiroishi, T., Ishino, F., and Kono, T. (1998) Disruption of primary imprinting during oocyte growth leads to the modified expression of imprinted genes during embryogenesis. *Development* **125,** 1553–1560
24. Coan, P. M., Burton, G. J., and Ferguson-Smith, A. C. (2005) Imprinted genes in the placenta. A review. *Placenta* **26,** S10–S20
25. Wu, X., Li, D. J., Yuan, M. M., Zhu, Y., and Wang, M. Y. (2004) The expression of CXCR4/CXCL12 in first-trimester human trophoblast cells. *Biol. Reprod.* **70,** 1877–1885
26. Mayer, W., Hemberger, M., Frank, H. G., Grümmer, R., Winterhager, E., Kaufmann, P., and Fundele, R. (2000) Expression of the imprinted genes MEST/Mest in human and murine placenta suggests a role in angiogenesis. *Dev. Dyn.* **217,** 1–10
27. Lefebvre, L., Viville, S., Barton, S. C., Ishino, F., Keverne, E. B., and Surani, M. A. (1998) Abnormal maternal behavior and growth retardation associated with loss of the imprinted gene Mest. *Nat. Genet.* **20,** 163–169

28. Looijenga, L. H., Gillis, A. J., Verkerk, A. J., van Putten, W. L., and Oosterhuis, J. W. (1999) Heterogeneous X inactivation in trophoblastic cells of human full-term female placentas. *Am. J. Hum. Genet.* **64,** 1445–1452
29. Beechey, C. V. (2000) Peg1/Mest locates distal to the currently defined imprinting region on mouse proximal chromosome 6 and identifies a new imprinting region affecting growth. *Cytogenet. Cell Genet.* **90,** 309–314
30. Nikonova, L., Koza, R. A., Mendoza, T., Chao, P. M., Curley, J. P., Kozak, L. P. (2008) Mesoderm-specific transcript is associated with fat mass expansion in response to a positive energy balance. *FASEB J.* **22,** 3925–3937
31. Lee, K. Y., Jeong, J. W., Tsai, S. Y., Lydon, J. P., and DeMayo, F. J. (2007) Mouse models of implantation. *Trends Endcrinol. Metab.* **18,** 234–239
32. Watson, E. D., and Cross, J. C. (2005) Development of structures and transport functions in the mouse placenta. *Physiology* **20,** 180–193
33. Chaddha, V., Viero, S., Huppertz, B., and Kingdom, J. (2004) Developmental biology of the placenta and the origins of placental insufficiency. *Semin. Fetal Neonatal Med.* **9,** 357–369
34. Migeon, B. R., Wolf, S. F., Axelman, J., Kaslow, D. C., and Schmidt, M. (1985) Incomplete X chromosome dosage compensation in chorionic villi of human placenta. *Proc. Natl. Acad. Sci. U.S.A.* **82,** 3390–3394
35. Coutinho-Camillo, C. M., Brentani, M. M., Butugan, O., Torloni, H., and Nagai, M. A. (2003) Relaxation of imprinting of IGFII gene in juvenile nasopharyngeal angiofibromas. *Diagn. Mol. Pathol.* **12,** 57–62
36. Sakatani, T., Wei, M., Katoh, M., Okita, C., Wada, D., Mitsuya, K., Meguro, M., Ikeguchi, M., Ito, H., Tycko, B., and Oshimura, M. (2001) Epigenetic heterogeneity at imprinted loci in normal populations. *Biochem. Biophys. Res. Commun.* **283,** 1124–1130
37. Bourdon, V., Philippe, C., Martin, D., Verloès, A., Grandemenge, A., and Jonveaux, P. (2003) MECP2 mutations or polymorphisms in mentally retarded boys. Diagnostic implications. *Mol. Diagn.* **7,** 3–7
38. Shahbazian, M. D., Sun, Y., and Zoghbi, H. Y. (2002) Balanced X chromosome inactivation patterns in the Rett syndrome brain. *Am. J. Med. Genet.* **111,** 164–168
39. Young, J. I., and Zoghbi, H. Y. (2004) X-chromosome inactivation patterns are unbalanced and affect the phenotypic outcome in a mouse model of rett syndrome. *Am. J. Hum. Genet.* **74,** 511–520
40. Kerr, B., Soto, C. J., Saez, M., Abrams, A., Walz, K., and Young, J. I. (2012) Transgenic complementation of MeCP2 deficiency. Phenotypic rescue of Mecp2-null mice by isoform-specific transgenes. *Eur. J. Hum. Genet.* **20,** 69–76